Available online at www.sciencedirect.com
SCIENCE DIRECT®
ELSEVIER
International Journal of Solids and Structures 42 (2005) 6141–6165
INTERNATIONAL JOURNAL OF SOLIDS and STRUCTURES
www.elsevier.com/locate/ijsolstr

Investigation of effective material properties in composites with internal defect or reinforcement particles

C.H. Yang [a], H. Huh [a,*], H.T. Hahn [b]

[a] *Department of Mechanical Engineering, Korea Advanced Institute of Science and Technology, 373-1 Kusong-dong, Yusong-gu, Science Town, Daejeon 305-701, Republic of Korea*
[b] *Department of Mechanical and Aerospace Engineering, UCLA, Los Angeles, CA 90095, USA*

Received 1 April 2004; received in revised form 22 June 2005
Available online 30 August 2005

Abstract

This paper is concerned with the investigation of the effective material properties of internally defective or particle-reinforced composites. An analysis was carried out with a novel method using the two-dimensional special finite element method mixing the concept of equivalent homogeneous materials. A formulation has been developed for a series of special finite elements containing an internal defect or reinforcement in order to assure the high accuracy especially in the vicinity of defects or reinforcements. The adoption of the special finite element can greatly simplify numerical modeling of particle-composites. The numerical result provides the effective material properties of particle-reinforced composite and explains that the size of particles has great influence on the material properties. Numerical examples also demonstrate the validity and versatility of the proposed method by comparing with existing results from literatures.

Keywords: Effective material property; Composite materials; Plane elasticity; Special FEM

1. Introduction

One of important research topics in composite materials is to study their effective material properties of composites (Christensen, 1979; Hasin, 1983; Vinson and Sierakowski, 1987; Gibson, 1994). Based on different assumptions, different averaging methods have been derived to obtain the effective elastic properties including differential method (Roscoe, 1952), composite spheres (cylinders) model (Hasin, 1962), self consistent method (Budiansky, 1965; Hill, 1965), generalized self consistent method (3-phase model;

* Corresponding author. Tel.: +82 42 869 3222; fax: +82 42 869 3210.
E-mail address: hhuh@kaist.ac.kr (H. Huh).

0020-7683/$ - see front matter © 2005 Elsevier Ltd. All rights reserved.
doi:10.1016/j.ijsolstr.2005.06.094

Christensen, 1979) and Mori–Tanaka method (Benveniste et al., 1989). Meguid and Kalamkarov (1994) developed an elastic homogenization model using the asymptotic homogenization technique.

The material properties of composites depend on the reinforced particles or fibers and are influenced by the internal defects or reinforcement particles with different sizes, materials and geometric distribution. The term as the size effect is used to describe such phenomena, which many engineering structures made of heterogeneous aggregate materials such as various particle-dispersed or fiber reinforced composites experience the variation in their global brittleness and strength as their size of internal defects or reinforcements increases. The elastic interaction of point defects was studied by Eshelby (1955) in addition to the elastic interaction between dislocations and point defects. Recently the researches on the size effect are also focused on the facture analysis on the micro-scale including Meng et al. (2001), Saouma et al. (2002), and Fischer et al. (2002). It is also found that such effects on nano-structured (nano-crystalline, nano-phase or nano-composite) materials are also of great importance from both fundamental considerations and modern practice. From the viewpoint of material science, Andrievski and Glezer (2001) summed up the recent progresses in material science on the study of the size effect on the material properties of nano-materials. However, it seems to be likely that the understanding of the nature of size effects on nano-structured materials is not so vivid that the possibility of the prediction in this field is still limited despite a great body of information. Up to now, nobody has noticed the size effect on effective material properties of composites induced by internal defects or reinforcements.

In order to study the problems about composite materials, the conventional FEM is not easy to be employed due to the complex stress fields involving stress concentration and singularity. Fortunately, a special 2-D finite element containing an internal defect or reinforcement has been well developed to assure the high precision in the vicinity of defects or reinforcements. The special element is constructed by using complex potentials to define the stress and displacement distribution functions (inter-polation functions) inside the element. There needs only one special element to simulate the surrounding zone of a defect or reinforcement and thus relatively simple and coarse mesh system can be used rather than a large number of conventional elements required in the conventional analysis. Because of the different techniques used to assure the displacement continuity along the inter-element boundary with other elements, the special finite element also has two types: the semi-analytic type and the hybrid type. The detailed construction procedure has been provided in other literatures (Tong et al., 1973; Tong, 1977; Piltner, 1985; Meguid and Zhu, 1995a,b; Zhang and Katsube, 1995a,b; Soh and Long, 1999, 2000; Yang and Soh, 2001; Yang et al., 2003; Soh and Yang, 2004) and their versatility and accuracy of the proposed special element also has been demonstrated with various examples.

In this paper, the above-mentioned two-dimensional semi-analytic special finite element method is employed to investigate the different effect including the size effect, material effect, distribution effect by internal particles as defect or reinforcement on the effective materials properties of composite panels using the concept of equivalent homogeneous materials under averaged displacements in their appropriate edges including the effective longitudinal/transverse Young's modulus, the shear modulus and the Poisson's ratio. In order to further simplify the numerical analysis and improve the calculation accuracy, the semi-analytic special element containing a circular hole or a circular elastic inhomogeneity has been reconstructed and a completely new semi-analytic special element containing a circular rigid inhomogeneity has been developed.

2. Two-dimensional special finite element method

2.1. The basics of special FEM

The two-dimensional special finite element method is termed as a kind of finite element which contains an internal inhomogeneity such as a hole, a crack, an elastic inhomogeneity and even a rigid inhomogene-

ity. Due to the implicit satisfaction of the boundary conditions in the vicinity of the internal inhomogeneity in advance, the kind of finite element can assure to obtain a high precision in the free or inter-facial boundaries within the elements. Most of all, there needs only one special element to simulate the surrounding zone of an inhomogeneity, and thus the relatively simple and coarse meshes can be used instead of a large number of conventional elements required. The computing time can be shortened greatly for complex problems of the complicated structures containing a large quantity of dispersed defects or reinforcements as well as composites.

The essence of the special finite element method is to use the complex potential method and conformal mapping technique developed by Muskhelishvili (1953) in defining the displacement and stress fields within the element. The defined displacement and stress fields as inter-polation functions must satisfy the boundary conditions simultaneously around the internal inhomogeneity. The conformal mapping technique is also employed to map the complicated internal boundaries inside the elements, such as the free boundary of a hole or crack and the inter-facial boundary between an inhomogeneity and a matrix, into a geometrically simpler boundary such as a unit circle for an original hole, a line for an original edge crack and a ring for an original inhomogeneity. Because of the different techniques used to assure the displacement continuity along the inter-element boundary S_C with other elements, the special finite elements also have two types: (a) semi-analytic type and (b) hybrid type.

2.2. A family of semi-analytic special finite elements

The present study considers only a series of the semi-analytic special finite elements as shown in Fig. 1 in which the special elements are reconstructed using a conforming mapping technique and further develops a completely new one containing an internal circular rigid inhomogeneity as shown in Fig. 1(c).

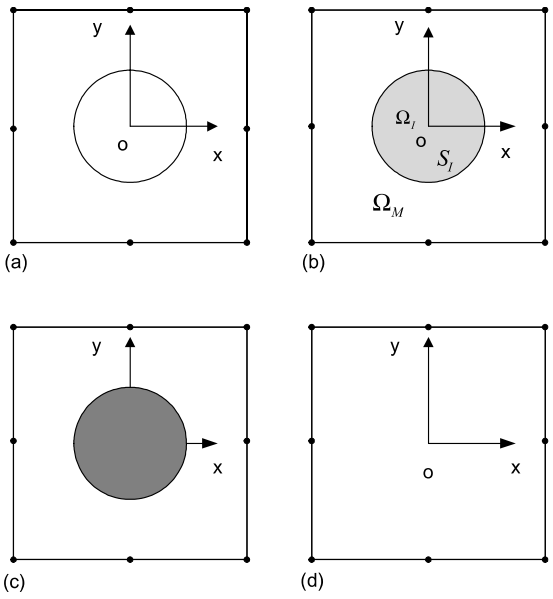

Fig. 1. A series of rectangular semi-analytic special elements: (a) 8-node special element with a circular hole, (b) 8-node special element with a circular elastic inhomogenity, (c) 8-node special element with a circular rigid inhomogenity, (d) 8-node degenerated special element.

In order to overcome the possible discontinuity of the displacement on the common boundary with conventional elements, a kind of degenerated special element is employed for the one containing an internal circular elastic inhomogeneity as shown in Fig. 1(d).

A typical special finite element shown in Fig. 1(b) has two internal regions: (a) an inhomogeneity (region Ω_I) and (b) a matrix (region Ω_M). For plane elasticity, the stress and displacement fields in these two internal regions can be well expressed in terms of the complex potentials $\Phi(z)$, $\psi(z)$ proposed by Muskhelishvili (1953) as follows:

$$\sigma_x + \sigma_y = 2\{\Phi'(z) + \overline{\Phi'(z)}\} \tag{1}$$

$$\sigma_x - \sigma_y + 2\mathrm{i}\tau_{xy} = 2\{\bar{z}\Phi''(z) + \psi'(z)\} \tag{2}$$

$$2\mu(u_x + \mathrm{i}u_y) = \kappa\Phi(z) - z\overline{\Phi'(z)} - \overline{\psi(z)} \tag{3}$$

$$F_x + \mathrm{i}F_y = -\mathrm{i}[\Phi(z) + z\overline{\Phi'(z)} + \overline{\psi(z)}]|_A^B = -\mathrm{i}[\Phi(z_B) + z_B\overline{\Phi'(z_B)} + \overline{\psi(z_B)} - C_A] \tag{4}$$

where $z = x + \mathrm{i}y$; μ is the shear modulus of a material; $\kappa = 3 - 4\nu$ for plane strain and $\kappa = \frac{3-\nu}{1+\nu}$ for plane stress, ν is the Poisson's ratio; A, B are the starting and end points of the integration; C_A is a complex constant at the datum point A; $'$ and $''$ denote the first and second-orders of complex differentiation with respect to z.

In order to improve the accuracy of calculation, the conformal mapping technique is then employed in the present special elements, such as the free boundary of a hole and the inter-facial boundary between an inhomogeneity and a matrix, to a unit circle. To consider the boundary as a circular hole with the radius ρ_0, the mapping function $f(\varsigma)$ can be given as

$$f(\varsigma) = \rho_0\varsigma \tag{5}$$

Further, the displacement and stress fields can be expressed in terms of $f(\varsigma)$ and the analytical functions $\Phi(\varsigma)$ and $\psi(\varsigma)$, which are chosen in the ς-plane as follows:

$$\sigma_x + \sigma_y = 2\left\{\frac{\Phi'(\varsigma)}{f'(\varsigma)} + \overline{\frac{\Phi'(\varsigma)}{f'(\varsigma)}}\right\} \tag{6}$$

$$\sigma_x - \sigma_y + 2\mathrm{i}\tau_{xy} = 2\left\{\overline{f(\varsigma)}\left(\frac{\Phi''(\varsigma)}{f'^2(\varsigma)} - \Phi'(\varsigma)\frac{f''(\varsigma)}{f'^3(\varsigma)}\right) + \frac{\psi'(\varsigma)}{f'(\varsigma)}\right\} \tag{7}$$

$$2\mu(u_x + \mathrm{i}u_y) = \kappa\Phi(\varsigma) - f(\varsigma)\overline{\frac{\Phi'(\varsigma)}{f'(\varsigma)}} - \overline{\psi(\varsigma)} \tag{8}$$

$$F_x + \mathrm{i}F_y = -\mathrm{i}\left[\Phi(\varsigma_{B'}) + f(\varsigma_{B'})\overline{\frac{\Phi'(\varsigma_{B'})}{f'(\varsigma_{B'})}} + \overline{\psi(\varsigma_{B'})} - C_{A'}\right] \tag{9}$$

where A' and B' are corresponding to the original integration points A and B; $C_{A'}$ is a complex constant. With the polar coordinates (ρ, θ) introduced in the transformed domain the above-mentioned relationships (5)–(8) can be rewritten as follows:

$$\sigma_\rho + \sigma_\theta = 2\left\{\frac{\Phi'(\varsigma)}{f'(\varsigma)} + \overline{\frac{\Phi'(\varsigma)}{f'(\varsigma)}}\right\} \tag{10}$$

$$\sigma_\theta - \sigma_\rho + 2\mathrm{i}\tau_{\rho\theta} = 2\mathrm{e}^{2\mathrm{i}\theta}\left\{\overline{f(\varsigma)}\left(\frac{\Phi''(\varsigma)}{f'^2(\varsigma)} - \Phi'(\varsigma)\frac{f''(\varsigma)}{f'^3(\varsigma)}\right) + \frac{\psi'(\varsigma)}{f'(\varsigma)}\right\} \tag{11}$$

$$2\mu(u_\rho + \mathrm{i}u_\theta) = \mathrm{e}^{-\mathrm{i}\theta}\left(\kappa\Phi(\varsigma) - f(\varsigma)\overline{\frac{\Phi'(\varsigma)}{f'(\varsigma)}} - \overline{\psi(\varsigma)}\right) \tag{12}$$

Different complex potentials $\Phi(\varsigma)$ and $\psi(\varsigma)$ are chosen for different forms of internal inhomogeneities as presented in Table 1. Table 2 presents various boundary conditions for different inhomogeneities embedded in the special finite elements. Substituting the complex potentials $\Phi(\varsigma)$ and $\psi(\varsigma)$ into the appropriate boundary conditions for different special elements and comparing the coefficients of various powers of $e^{i\theta}$, the different relation between the coefficients in them can be deduced. Thus, the independent coefficients can be determined since their number is exactly equal to the total number of degrees-of-freedom in the nodes of the element.

Noting that in the case of an elastic inhomogeneity deduced by Meguid and Zhu (1995a,b), the null is not appropriate to set the independent coefficients H_1, M_1 and D_1 because of lacking these important second-order terms of z in the potential functions, the related element becomes stiffer, especially in the cases with big inhomogeneity.

Table 1
The complex potentials $\Phi(\varsigma)$, $\psi(\varsigma)$ for different inhomogeneities

No.	Inhomogeneities	Potentials $\Phi(\varsigma)$, $\psi(\varsigma)$
1	An internal circular hole	$\Phi(\varsigma) = \Phi_0 + \sum_{k=1}^{k_U} A_k \varsigma^k + \sum_{l=1}^{l_U} B_l \varsigma^{-l}$
		$\psi(\varsigma) = \psi_0 + \sum_{m=1}^{m_U} C_m \varsigma^m + \sum_{n=1}^{n_U} D_n \varsigma^{-n}$ at $\lvert\varsigma\rvert \geqslant 1.0$
2	An internal circular elastic inhomogeneity	$\Phi_M(\varsigma) = \Phi_{M0} + \sum_{k=1}^{k_U} A_k \varsigma^k + \sum_{l=1}^{l_U} B_l \varsigma^{-l}$
		$\psi_M(\varsigma) = \psi_{M0} + \sum_{m=1}^{m_U} C_m \varsigma^m + \sum_{n=1}^{n_U} D_n \varsigma^{-n}$ at $\lvert\varsigma\rvert \geqslant 1.0$
		$\Phi_I(\varsigma) = \Phi_{I0} + \sum_{p=1}^{p_U} E_p \varsigma^p$
		$\psi_I(\varsigma) = \psi_{I0} + \sum_{p=1}^{p_U} F_p \varsigma^p$ at $0 < \lvert\varsigma\rvert < 1.0$
3	An internal circular rigid inhomogeneity	$\Phi_M(\varsigma) = \Phi_{M0} + \sum_{k=1}^{k_U} A_k \varsigma^k + \sum_{l=1}^{l_U} B_l \varsigma^{-l}$
		$\psi_M(\varsigma) = \psi_{M0} + \sum_{m=1}^{m_U} C_m \varsigma^m + \sum_{n=1}^{n_U} D_n \varsigma^{-n}$ at $\lvert\varsigma\rvert \geqslant 1.0$

Table 2
Various boundary conditions for different inhomogeneities

No.	Inhomogeneities	Boundary conditions
1	An internal circular hole	The traction-free conditions on the crack surface: $\sigma_\rho = \tau_{\rho\theta} = 0$, in the ς-plane and $F_x = F_y = 0$, in the z-plane
2	An internal circular elastic inhomogeneity	The inter-facial boundary conditions for perfect bonding: $(F_x + iF_y)_M = (F_x + iF_y)_I$ and $(u + iv)_M = (u + iv)_I$ in the z-plane
3	An internal circular rigid inhomogeneity	The inter-facial boundary conditions for perfect bonding: $(u + iv)\lvert_M = u_0 + i(v_0 - \theta_0 e^{i\theta})$ and $F_x = F_y = 0$ in the z-plane, where u_0, v_0 and θ_0 are rigid-body displacements and rotation angle

After using Eq. (8) for different internal regions within a typical special element containing an elastic inhomogeneity,

$$\mathbf{U}_M = \begin{Bmatrix} u_{Mx} \\ v_{My} \end{Bmatrix} = \mathbf{\Omega}_M \mathbf{q}_M \quad \text{in } \Omega_M \tag{13}$$

$$\mathbf{U}_I = \begin{Bmatrix} u_I \\ v_I \end{Bmatrix} = \mathbf{\Omega}_I \mathbf{q}_I \quad \text{in } \Omega_I \tag{14}$$

where $\mathbf{q}_M$ and $\mathbf{q}_I$ are the column matrices consisting of the unknown complex coefficients in the regions Ω_M and Ω_I, respectively; $\mathbf{\Omega}_M$ and $\mathbf{\Omega}_I$ are the corresponding displacement matrices as $\mathbf{\Omega}_M = \{\, \mathbf{\Omega}_{Mx} \quad \mathbf{\Omega}_{My} \,\}^{\mathrm{T}}$, $\mathbf{\Omega}_I = \{\, \mathbf{\Omega}_{Ix} \quad \mathbf{\Omega}_{Iy} \,\}^{\mathrm{T}}$.

Further, Eq. (14) can be rewritten as

$$\{\mathbf{U}_I\} = \begin{Bmatrix} u_I \\ v_I \end{Bmatrix} = [\mathbf{\Omega}_I]\{\mathbf{q}_I\} = [\mathbf{\Omega}_I][\mathbf{T}_q]\{\mathbf{q}_M\} \quad \text{in } \Omega_I \tag{15}$$

where $[\mathbf{T}_q]$ is the relationship matrix between $\{\mathbf{q}_M\}$ and $\{\mathbf{q}_I\}$.

The nodal displacement vector $\{\mathbf{U}\}^{\mathrm{e}}$ of a rectangular 8-node element is defined as

$$\{\mathbf{U}\}^{\mathrm{e}} = [\,(u)_1 \quad (v)_1 \quad (u)_2 \quad (v)_2 \quad \cdots \quad (u)_8 \quad (v)_8\,]^{\mathrm{T}} \tag{16}$$

where $(u)_i$ and $(v)_i$ are the x and y displacement components of node i ($i = 1, \ldots, 8$), respectively. Substituting the nodal displacements at all the eight nodal points of the element into Eq. (13), we obtain

$$\{\mathbf{U}\}^{\mathrm{e}} = [\mathbf{\Omega}_M^{\mathrm{e}}]\{\mathbf{q}_M\} \tag{17}$$

where $[\mathbf{\Omega}_M^{\mathrm{e}}] = \{\, (\mathbf{\Omega}_{Mx})_1 \quad (\mathbf{\Omega}_{My})_1 \quad (\mathbf{\Omega}_{Mx})_2 \quad (\mathbf{\Omega}_{My})_2 \quad \cdots \quad (\mathbf{\Omega}_{Mx})_8 \quad (\mathbf{\Omega}_{My})_8 \,\}^{\mathrm{T}}$

Further,

$$\{\mathbf{q}_M\} = [\mathbf{\Omega}_M^{\mathrm{e}}]^{-1}\{\mathbf{U}\}^{\mathrm{e}} \tag{18}$$

Substituting Eq. (18) into Eqs. (13) and (14), the displacement fields at any point within the element can be expressed in terms of the nodal displacement vectors as follows:

$$\{\mathbf{U}_M\} = \begin{Bmatrix} u_M \\ v_M \end{Bmatrix} = [\mathbf{\Omega}_M][\mathbf{\Omega}_M^{\mathrm{e}}]^{-1}\{\mathbf{U}^{\mathrm{e}}\} = [\mathbf{N}_M]\{\mathbf{U}^{\mathrm{e}}\} \tag{19}$$

$$\{\mathbf{U}_I\} = \begin{Bmatrix} u_I \\ v_I \end{Bmatrix} = [\mathbf{\Omega}_I][\mathbf{T}_\beta][\mathbf{\Omega}_M^{\mathrm{e}}]^{-1}\{\mathbf{U}^{\mathrm{e}}\} = [\mathbf{N}_I]\{\mathbf{U}^{\mathrm{e}}\} \tag{20}$$

where $[N_M]_{2\times 2n} = [\mathbf{\Omega}_M][\mathbf{\Omega}_M^{\mathrm{e}}]^{-1}$ and $[N_I]_{2\times 2n} = [\mathbf{\Omega}_I][\mathbf{T}_\beta][\mathbf{\Omega}_M^{\mathrm{e}}]^{-1}$ are the element shape functions according to the conventional FEM.

According to the standard finite element approach, the strain vectors $\boldsymbol{\varepsilon}_M$ and $\boldsymbol{\varepsilon}_D$ at any point inside the element can be obtained as follows:

$$\{\boldsymbol{\varepsilon}_M\} = \begin{Bmatrix} \varepsilon_{Mx} \\ \varepsilon_{My} \\ \varepsilon_{Mxy} \end{Bmatrix} = \begin{bmatrix} \dfrac{\partial}{\partial x} & 0 \\ 0 & \dfrac{\partial}{\partial y} \\ \dfrac{\partial}{\partial y} & \dfrac{\partial}{\partial x} \end{bmatrix} \quad \{\mathbf{U}\} = \begin{bmatrix} \dfrac{\partial \mathbf{\Omega}_{Mx}}{\partial x} \\ \dfrac{\partial \mathbf{\Omega}_{My}}{\partial y} \\ \dfrac{\partial \mathbf{\Omega}_{Mx}}{\partial y} + \dfrac{\partial \mathbf{\Omega}_{My}}{\partial x} \end{bmatrix} [\mathbf{\Omega}_M^{\mathrm{e}}]^{-1} \quad \{\mathbf{U}^{\mathrm{e}}\} = [\mathbf{B}_M]\{\mathbf{U}^{\mathrm{e}}\} \tag{21}$$

$$\{\boldsymbol{\varepsilon}_I\} = \begin{Bmatrix} \varepsilon_{Ix} \\ \varepsilon_{Iy} \\ \gamma_{Ixy} \end{Bmatrix} = \begin{bmatrix} \dfrac{\partial}{\partial x} & 0 \\ 0 & \dfrac{\partial}{\partial y} \\ \dfrac{\partial}{\partial y} & \dfrac{\partial}{\partial x} \end{bmatrix} \quad \{\mathbf{U}\} = \begin{bmatrix} \dfrac{\partial \boldsymbol{\Omega}_{Ix}}{\partial x} \\ \dfrac{\partial \boldsymbol{\Omega}_{Iy}}{\partial y} \\ \dfrac{\partial \boldsymbol{\Omega}_{Ix}}{\partial y} + \dfrac{\partial \boldsymbol{\Omega}_{Iy}}{\partial x} \end{bmatrix} [\boldsymbol{\Omega}_M^{\mathrm{e}}]^{-1} \quad \{\mathbf{U}^{\mathrm{e}}\} = [\mathbf{B}_I]\{\mathbf{U}^{\mathrm{e}}\} \tag{22}$$

where $[\mathbf{B}_M]$ and $[\mathbf{B}_I]$ are the so-called element strain-displacement matrices.

Directly from the nodal force equilibrium,

$$\int\int_{A^{\mathrm{e}}} [\mathbf{B}]^{\mathrm{T}}[\boldsymbol{\sigma}] dA^{\mathrm{e}} = [\mathbf{F}] \tag{23}$$

where **B** and **F** are stress and nodal force vectors, respectively. If the stress vector in (23) is replaced by the strain vector and the elastic matrix **D**, we have

$$\left[\int\int_{A^{\mathrm{e}}} [\mathbf{B}]^{\mathrm{T}}[\mathbf{D}][\mathbf{B}]\,\mathrm{d}A^{\mathrm{e}}\right]\{\mathbf{q}^{\mathrm{e}}\} = \{\mathbf{F}\} \quad \text{or} \quad [K]_{\mathrm{s}}^{\mathrm{e}}\{\mathbf{q}^{\mathrm{e}}\} = \{\mathbf{F}\} \tag{24}$$

Thus, considering the different parts of special elements occupied by different materials, the element stiffness matrix can be deduced as

$$[\mathbf{K}]_{\mathrm{s}}^{\mathrm{e}} = \int_{A^{\mathrm{e}}} [\mathbf{B}]^{\mathrm{T}}[\mathbf{D}][\mathbf{B}] t\,\mathrm{d}A^{\mathrm{e}} = \int\int_{A_M} [\mathbf{B}_M]^{\mathrm{T}}[\mathbf{D}_M][\mathbf{B}_M] t\,\mathrm{d}A_M + \int\int_{A_I} [\mathbf{B}_I]^{\mathrm{T}}[\mathbf{D}_I][\mathbf{B}_I] t\,\mathrm{d}A_I \tag{25}$$

where $[\mathbf{D}_M]$ and $[\mathbf{D}_I]$ are the element elasticity matrices; t is the plate thickness; A^{e}, A_M and A_I are the area of the whole element, the area of its matrix part and the area of its inhomogeneity part, and $A^{\mathrm{e}} = A_M + A_I$. Noting that as for the cases the special element containing a hole or a rigid inhomogeneity, the element stiffness matrix should be degenerated as

$$[\mathbf{K}]_{\mathrm{s}}^{\mathrm{e}} = \int_{A^{\mathrm{e}}} [\mathbf{B}]^{\mathrm{T}}[\mathbf{D}][\mathbf{B}] t\,\mathrm{d}A^{\mathrm{e}} \tag{26}$$

where $[\mathbf{D}] = [\mathbf{D}_M]$; $[\mathbf{B}] = [\mathbf{B}_M]$; $A^{\mathrm{e}} = A_M$.

On the basis of degenerated element according to Eq. (25), the degenerated homogeneous element can be also developed by setting $A_I = 0$ or $\mathbf{D}_M = \mathbf{D}_I$ and this element will have the same displacement distribution along their common boundary with the corresponding special elements and thus there will be no such problems of possible displacement discontinuity along the inter-element boundaries in the FE models using special finite elements mixed with degenerated homogeneous elements.

2.3. Comparison between the different semi-analytic special elements proposed

All of three above-mentioned special elements will be employed in the present numerical analysis. Even though the hole and the rigid inhomogeneity can be regarded as two extreme cases of the elastic inhomogeneity, the special element containing an inhomogeneity cannot properly replace the other two ones by setting the extreme values of the material properties of the internal inhomogeneity as $G = 0$ and $G = \infty$. According to Eq. (25), the quantity scale of G and μ_I or E_I will keep the same and thus the second term in the right side of Eq. (25) will not disappear automatically. In another word, even though a relatively small or big number of μ_I or E_I can be set very well, we still cannot obtain the more accurate solutions in the cases of the hole and the rigid inhomogeneity using Eq. (25) due to its harder element stiffness.

For an example, a square panel is considered with a circular hole, a circular elastic homogeneity and a rigid homogeneity subjected to uniaxial tension in the y-direction, their stresses at $\theta = 0°$ and 90° and

Table 3
Results of stresses along the internal boundaries using different special finite element ($\rho_0 = 0.25$, $a = b = 20$, $\sigma_0 = 1$, $E_M = 100$, $\upsilon_M = 0.3$)

No.	Cases	$\sigma_\rho/\sigma_\theta$	θ (°)	
			0	90
1	Circular hole	σ_ρ	0	0
		σ_θ	3.0830	−1.0349
	Circular elastic inhomogeneity ($E_I = 1 \times 10^{-6}$, $\upsilon_I = 0$)	σ_ρ	0	0
		σ_θ	3.0010	−1.0006
	Exact solutions	σ_ρ	0	0
		σ_θ	3.0000	−1.0000
2	Circular elastic inhomogeneity ($E_I = 1 \times 10^{9}$, $\upsilon_I = 0$)	σ_ρ	−0.03311	1.4767
		σ_θ	−0.07727	0.6329
	Circular rigid inhomogeneity	σ_ρ	−0.03312	1.4767
		σ_θ	−0.07727	0.6329
	Exact solution	σ_ρ	−0.03333	1.4778
		σ_θ	−0.07778	0.6333

deformations have been compared with each other. As presented in Table 3, all of three special elements can assure good solutions of stresses along the internal boundaries while the special element containing an elastic inhomogeneity at two approximately extreme cases for the other two cannot assure reasonable results for displacements. Moreover, as for these two special finite elements containing an internal hole or a rigid inhomogeneity, the calculation of element stiffness matrixes needs only integration in the matrix part and thus it reduces the CPU time greatly. That is why two special finite elements containing an internal hole or a rigid inhomogeneity have been specially developed.

3. Effective material properties of composites

3.1. Material properties of composite materials

In order to consider a composite with randomly-dispersed particles or a cross-section of fiber reinforced composite as shown in Fig. 2, the composite material can be regarded as a typical anisotropic material in a simple two-dimensional state of stress or strain. For the sake of simplicity of the corresponding analyses, only a series of square composite panels are considered.

According to the anisotropic stress–strain relationships in the principal material coordinates, there are only six independent material constants such as the longitudinal modulus E_1, the transverse modulus E_2,

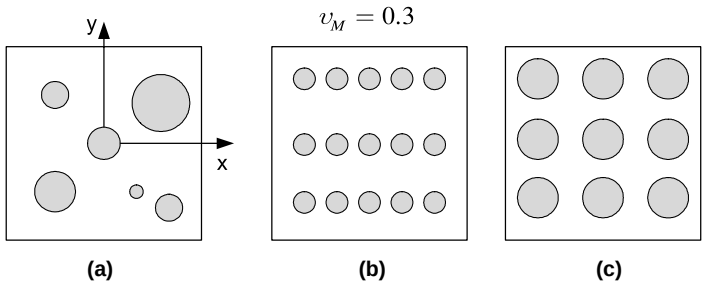

Fig. 2. The mathematical models of a square composite panel.

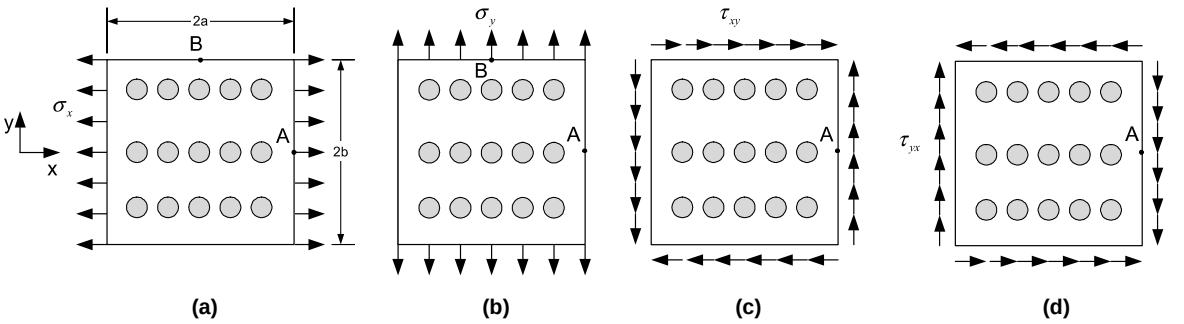

Fig. 3. The mathematical models to define the material properties of composites.

the major shear modulus G_{12}, the minor shear modulus G_{21}, the major Poisson's ratio v_{12}, and the minor Poisson's ratio v_{21}. Further as the case shown in Fig. 2(c), if the distributions of the internal defects or reinforcements are evenly both in x- and y-direction, only three material constants of the Young's modulus $E_1 = E_2$, the shear modulus $G_{12} = G_{21}$ and the Poisson's ratio $v_{12} = v_{21}$ are independent.

In order to determine the above-mentioned material constants, different mathematical models are needed as shown in Fig. 3(a)–(d).

3.2. Effective properties of equivalent homogeneous materials

The concept of the equivalent homogeneous materials under averaged displacement is introduced to scale the material properties of the plates containing different inhomogeneity. The equivalent homogeneous material has the same geometrical dimensions as the original one but without any inhomogeneities and thus it has different material properties. Its effective material properties, including the effective elastic modulus E_e, Poisson's ratio v_e and shear modulus G_e have been introduced and they can be calculated with the corresponding theory from the so-called averaged displacements and rotation angle $\bar{u}$, $\bar{v}$and $\bar{\delta}$ along the different, appropriate edges of big plates. According to the related theory of plane elasticity (Timoshenko and Goodier, 1970), to consider the plane stress problem of a big plate without any inhomogeneities under uniaxial tension, the related Airy stress functions can be given as

$$\begin{cases} \psi_1 = \dfrac{1}{2}\sigma_1 y^2 \\ \psi_2 = \dfrac{1}{2}\sigma_2 x^2 \\ \psi_3 = \dfrac{1}{2}\tau_{12} xy \\ \psi_4 = -\dfrac{1}{2}\tau_{21} xy \end{cases} \tag{27}$$

which obviously satisfies the biharmonic equation $\nabla^2\psi_i = 0$, $i = 1, 2, 3, 4$; $\sigma_1 = \sigma_x$, $\sigma_2 = \sigma_y$, $\tau_{12} = \tau_{xy}$ and $\tau_{21} = \tau_{yx}$.

After applying the stress–displacement relationship of plane problem, the displacement fields of a plate under uniaxial tension in the x- or y-direction in plane stress and plane strain are obtained as follows, respectively,

$$\begin{cases} u_1 = \dfrac{1}{E}\sigma_1 x \\ v_1 = -\dfrac{v}{E}\sigma_1 y \end{cases} \tag{28}$$

$$\begin{cases} u_2 = -\dfrac{v}{E}\sigma_2 x \\ v_2 = \dfrac{1}{E}\sigma_2 y \end{cases} \tag{29}$$

or

$$\begin{cases} u_1 = \dfrac{1}{E}(1-v^2)\sigma_1 x \\ v_1 = -\dfrac{1}{E}(1+v)v\sigma_1 y \end{cases} \tag{30}$$

$$\begin{cases} u_2 = -\dfrac{1}{E}(1+v)v\sigma_2 x \\ v_2 = \dfrac{1}{E}(1-v^2)\sigma_2 y \end{cases} \tag{31}$$

Further to calculate the effective longitudinal elastic Young's moduli E_e^i, $i = 1, 2$ and Poisson's ratio v_e^i, $i = 1, 2$, the corresponding reference points A, (a, 0) and B, (0, b) are selected. The averaged displacements $\bar{u}_A$ and $\bar{v}_A$ at x- and y-directions along the edge with point A, and $\bar{u}_B$ and $\bar{v}_B$ at x- and y-directions along another edge with B can be calculated from the above-mentioned finite element models using special finite element in the previous section. So, for plane stress problems

$$\begin{cases} E_e^1 = \dfrac{1}{\bar{u}_A}\sigma_1 a \\ v_e^1 = -\dfrac{\bar{v}_B E_e^1}{\sigma_1 b} \end{cases} \tag{32}$$

$$\begin{cases} E_e^2 = \dfrac{1}{\bar{v}_B}\sigma_2 b \\ v_e^2 = -\dfrac{\bar{u}_A E_e^2}{\sigma_2 a} \end{cases} \tag{33}$$

and, for plane strain problems,

$$\begin{cases} v_e^1 = \dfrac{1}{1+\left|\dfrac{\bar{u}_A}{\bar{v}_B}\right|\dfrac{b}{a}} \\ E_e^1 = \dfrac{1}{\bar{u}_A}[1-(v_e^1)^2]\sigma_1 a \quad \text{or} \quad E_e^1 = -\dfrac{1}{\bar{v}_B}(1+v_e^1)v_e^1\sigma_1 b \end{cases} \tag{34}$$

$$\begin{cases} v_e^2 = \dfrac{1}{1+\left|\dfrac{\bar{v}_B}{\bar{u}_A}\right|\dfrac{a}{b}} \\ E_e^2 = \dfrac{1}{\bar{v}_B}[1-(v_e^2)^2]\sigma_2 b \quad \text{or} \quad E_e^2 = -\dfrac{1}{\bar{u}_A}(1+v_e^2)v_e^2\sigma_2 a \end{cases} \tag{35}$$

As the cases under shear loads shown in Fig. 8(c) and (d), the effective in-plane shear moduli can be calculated directly according to the following formulas

$$G_{\mathrm{e}}^{12} = \frac{\bar{\tau}_{12}}{\bar{\gamma}_{12}} \tag{36}$$

and

$$G_{\mathrm{e}}^{21} = \frac{\bar{\tau}_{21}}{\bar{\gamma}_{21}} \tag{37}$$

where $\bar{\tau}_{12}$ and $\bar{\tau}_{21}$ are the average composite shear stresses in the 12 and 21 planes over the edge with point A, respectively; $\bar{\gamma}_{12} = 2\bar{\varepsilon}_{12}$ and $\bar{\gamma}_{21} = 2\bar{\varepsilon}_{21}$ are the average engineering shear strains in the 12 and 21 planes over the edge with point A, respectively.

3.3. Bounds of effective material properties

According to the basic ideas and methods in mechanics of composite materials, the corresponding upper and lower bounds of the effective material properties also can be calculated through the above-mentioned method by selecting those appropriate points in the appropriate edges, which have the minimum and maximum values of displacements u and v in different directions. Thus, the upper bound of the effective elastic module E_{e} and Poisson's ratio v_{e} can be obtained,

$$E_{\mathrm{e}}^{\mathrm{U}} = \frac{1}{u_{\mathrm{MIN}}}\sigma_0 a \tag{38}$$

$$v_{\mathrm{e}}^{\mathrm{U}} = -\frac{v_{\mathrm{MIN}} E_{\mathrm{e}}}{\sigma_0 b} \tag{39}$$

and

$$v_{\mathrm{e}}^{\mathrm{U}} = \frac{1}{1 - \frac{u_{\mathrm{MIN}}}{v_{\mathrm{MIN}}}\frac{b}{a}} \tag{40}$$

$$E_{\mathrm{e}}^{\mathrm{U}} = \frac{1}{u_{\mathrm{MIN}}}(1 - v_{\mathrm{e}}^2)\sigma_0 a \tag{41}$$

or

$$E_{\mathrm{e}}^{\mathrm{U}} = -\frac{1}{v_{\mathrm{MIN}}}(1 + v_{\mathrm{e}})v_{\mathrm{e}}\sigma_0 b \tag{42}$$

and further, the lower bound of the effective elastic module E_{e} and Poisson's ratio v_{e} can be obtained too, respectively,

$$E_{\mathrm{e}}^{\mathrm{L}} = \frac{1}{u_{\mathrm{MAX}}}\sigma_0 a \tag{43}$$

$$v_{\mathrm{e}}^{\mathrm{L}} = -\frac{v_{\mathrm{MAX}} E_{\mathrm{e}}}{\sigma_0 b} \tag{44}$$

and

$$v_{\mathrm{e}}^{\mathrm{L}} = \frac{1}{1 - \frac{u_{\mathrm{MAX}}}{v_{\mathrm{MAX}}}\frac{b}{a}} \tag{45}$$

$$E_{\mathrm{e}}^{\mathrm{L}} = \frac{1}{u_{\mathrm{MAX}}}(1 - v_{\mathrm{e}}^2)\sigma_0 a \tag{46}$$

or

$$E_{\mathrm{e}}^{\mathrm{L}} = -\frac{1}{v_{\mathrm{MAX}}}(1 + v_{\mathrm{e}})v_{\mathrm{e}}\sigma_0 b \tag{47}$$

As for shear modulus, the bounds of effective in-plane shear moduli can be calculated directly according to the following formulas:

$$G_e^U = \frac{\bar{\tau}_{12\,MIN}}{\bar{\gamma}_{12\,MIN}} \tag{48}$$

and

$$G_e^L = \frac{\bar{\tau}_{12\,MAX}}{\bar{\gamma}_{12\,MAX}} \tag{49}$$

Thus, on the basis of the averaged displacements/strains along the appropriate edges of a composite panel from FE models, all its elastic material constants and even their bounds can be determined.

4. Numerical examples

4.1. Finite element models using defect/reinforcement finite elements

In order to consider a series of big plates with different inhomogeneities subjected to uniaxial tension, their corresponding 2-D linear finite element models with coarse meshes using 8-node special elements have been built up and shown in Figs. 4 and 5. Note that, only the special elements are used in the finite element

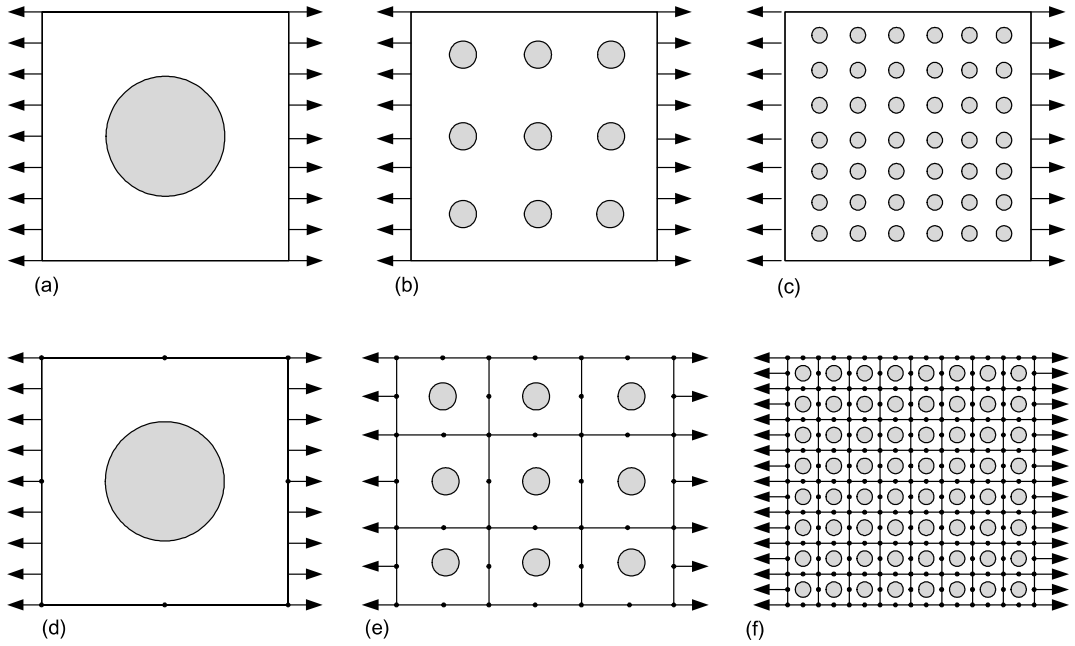

Fig. 4. A series of square panels with uniformly-distributed internal inhomogeneities at different scales and their finite element meshes using 8-node defect/reinforcement finite elements: (a) square panel with one defect/reinforcement, (b) a square panel with multiple defects/reinforcements, (c) a square panel with a lot of small defects/reinforcements, (d) FE mesh of a square panel with one defect/reinforcement, (e) FE mesh of a square panel with multiple defects/reinforcements, (f) FE mesh of a square panel with a lot of small defects/reinforcements.

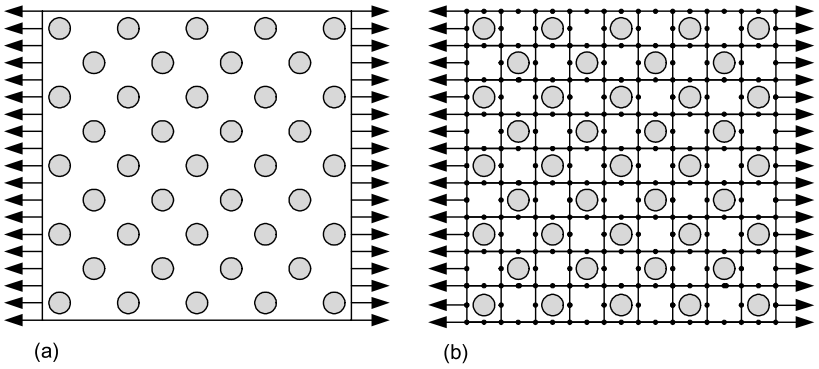

Fig. 5. A series of panels with internal inhomogeneities and their finite element meshes using 8-node defect/reinforcement finite elements: (a) a square panel with multiple defects/reinforcements, (b) FE mesh of a square panel with multiple defects/reinforcements.

meshes and thus these models are easy to generate even in the case of those plates with a large amount of internal inhomogeneities.

As for the different cases of the plates with the different numbers of the internal defects/reinforcements, their numbers has been set appropriately to assure the volume fraction γ as a constant or a variable. At the present analysis, the amounts of the internal inhomogeneities are varied from 1×1, 3×3, 5×5, 10×10, 20×20, 50×50, and 100×100 (uniformly distributed) or 16 and 41 (not uniformly distributed). In all cases, the numbers of the internal inhomogeneities are exactly equal to those of special elements in the present models just because there is only one special element needed to simulate the vicinity of an inhomogeneity. Note that in the case of a large amount of inhomogeneities, it is almost impossible to generate the corresponding finite element models to process the same analysis using conventional elements for such complicated problems related to stress concentration or stress singularity.

For the sake of simplicity of these analyses, the internal inhomogeneities are arranged evenly and the internal inhomogeneities are only in the form of a circular hole, circular elastic inhomogeneity including two cases, defect or reinforcement, and circular rigid inhomogeneity. Although the corresponding 2-D problems of a particle-dispersed composite material should be regarded as a plane stress problem and those about the fiber composite materials should be treated as a plane strain problem, only the plane strain problem is to be analyzed in the present studies.

In all the present plane strain analyses of large plates with different inhomogeneities, the geometrical parameter of the plates is 20×20 or 40×20 (length $\times$ width), and the remote uniform stress applied was $\sigma_0=1$ along one edge of these plates in the horizontal direction. The material constants of the surrounding matrix in all large plates were assumed to be $E_M=1$ and $v_M=0.3$, and it just needs to adjust the elastic modulus E_I of the elastic inhomogeneity and further obtain the different shear modulus ratio $\Gamma=\frac{\mu_I}{\mu_M}$ of the inhomogeneity and the matrix if need. As for the material properties of different inhomogeneities as circular elastic inhomogeneities, they have different values in the two cases: (a) defect (soft inhomogeneity), Γ is selected as 0.5; and (b) reinforcement (stiff inhomogeneity), it is set to 5 and 50, respectively.

4.2. Size effects of internal particles in a series of big composite panels

4.2.1. Size effects with different volume fractions between inhomogeneities and matrix

The size effect of internal particles is considered to demonstrate the validity of the above-mentioned finite element model designed using defect/reinforcement finite elements in some cases of fiber-composite materials with the different volume fraction. First, the analysis considers the case with 1×1 inhomogeneity

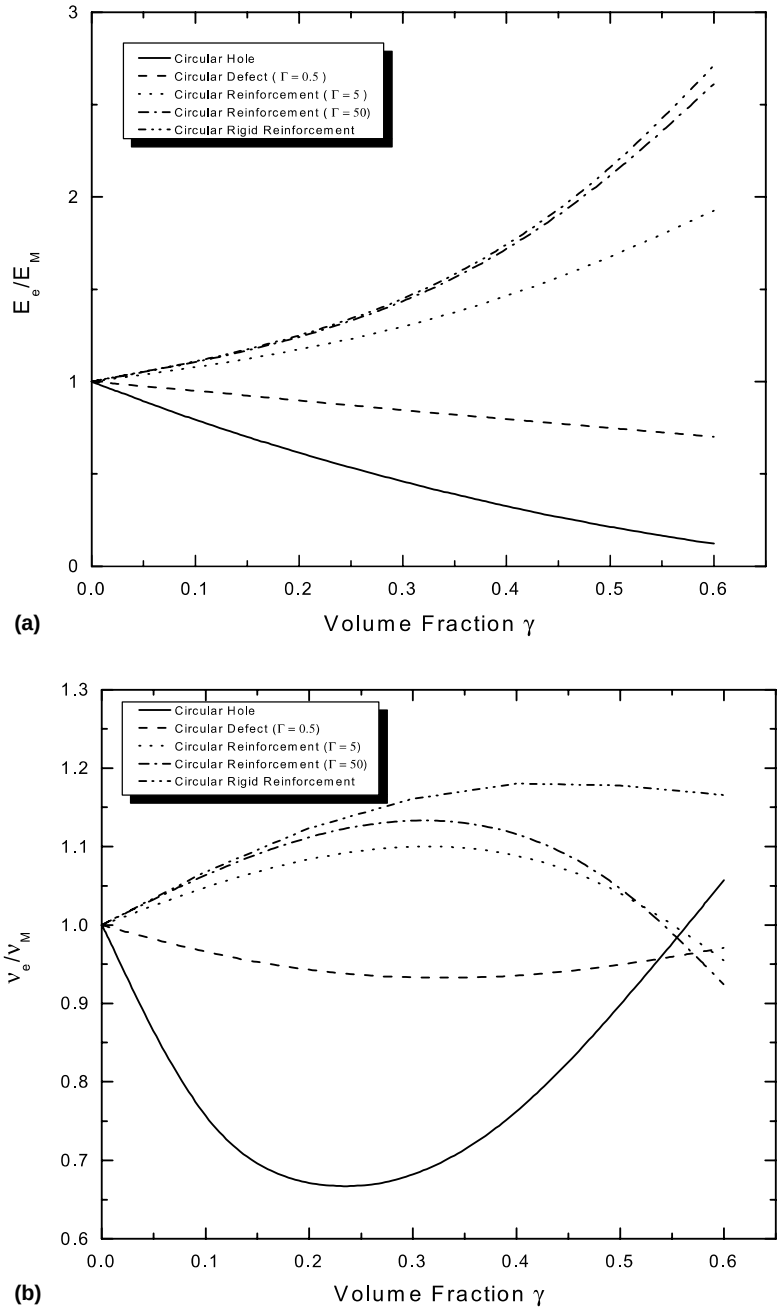

Fig. 6. Numerical results of the effective Young's ratio E_e/E_M and Poisson's ratio v_e/v_M of the plates containing an inhomogeneity versus different volume fraction γ: (a) E_e/E_M, (b) v_e/v_M.

shown in Fig. 4(d). The corresponding results are given in Fig. 6(a) and (b) for the effective elastic modulus ratio E_e/E_M and the effective Poisson's ratio v_e/v_M of the plates containing only one defect/reinforcement with varying the volume fraction γ.

Secondly, in order to demonstrate the validity of the present finite element models, the case with 3×3 inhomogeneities are selected with the same material properties and the distribution of reinforcements given by Meguid and Zhu (1995a,b) as shown in Fig. 4(e). Numerical results of the effective material properties including the effective elastic modulus ratio E_e/E_M are compared with those from analytical procedures including an extreme solution provided by Christensen (1990), an analytical solution obtained by Meguid and Kalamkarov (1994) using the technique of asymptotic homogenization, and the numerical solutions by Meguid and Zhu (1995a,b), as shown in Fig. 7 that explains the validity of the solutions and the numerical results obtained using the present reconstructed special element are in good agreement with the low bound at the small volume fraction ($\gamma = 0.4$).

The corresponding results are given in Figs. 8–11 for both the effective elastic modulus ratio E_e/E_M and the effective Poisson's ratio v_e/v_M of the plates containing multiple inhomogeneities of 3×3, 10×10, 20×20 and 100×100 with the variation of the volume fraction γ. In these above-mentioned cases, the internal inhomogeneities are distributed uniformly and thus only three material constants are independent such as Young's modulus $E_1 = E_2$, shear modulus $G_{12} = G_{21}$, Poisson's ratio $v_{12} = v_{21}$. From these numerical results, the arrangement of internal inhomogeneities will greatly influence the mechanical behavior of the whole composite material and the effective Poisson's ratio varies greatly with different arrangements of internal inhomogeneities while the effective Young's modulus is insensitive.

In other cases of a square panel as given in Fig. 5(b), the arrangement of internal inhomogeneities is not evenly distributed along both the x- and y-directions and their effective longitudinal elastic modulus ratio E_e/E_M and Poisson's ratio v_e/v_M with the variation of the volume fraction γ are given in Fig. 12.

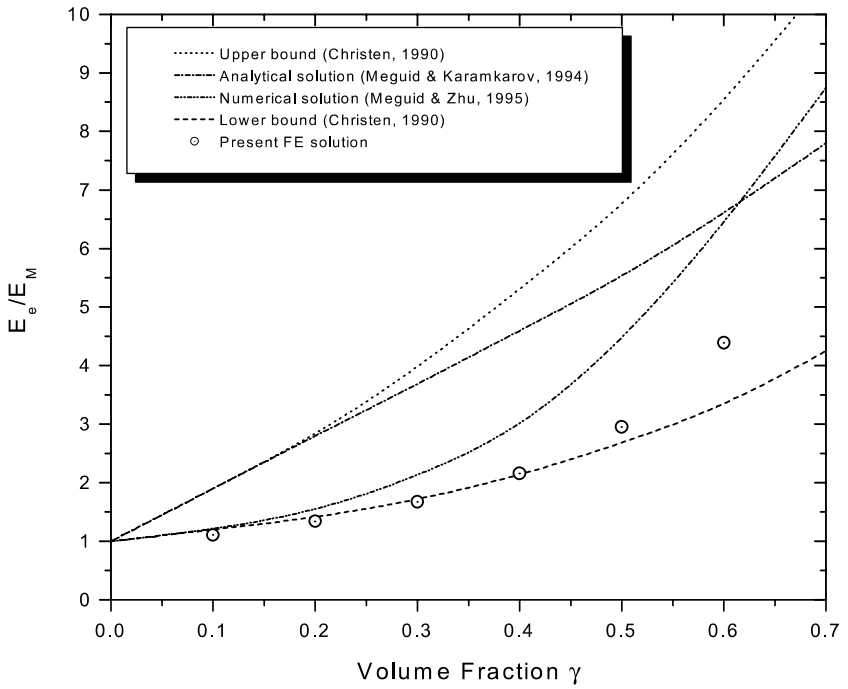

Fig. 7. Comparison of the numerical results of effective elastic modulus ratio E_e/E_M of the plates containing 9 (3×3) inhomogeneities versus different volume fraction γ ($E_R = 73$ GPa, $v_R = 0.23$ and $E_M = 3.43$ GPa, $v_M = 0.35$).

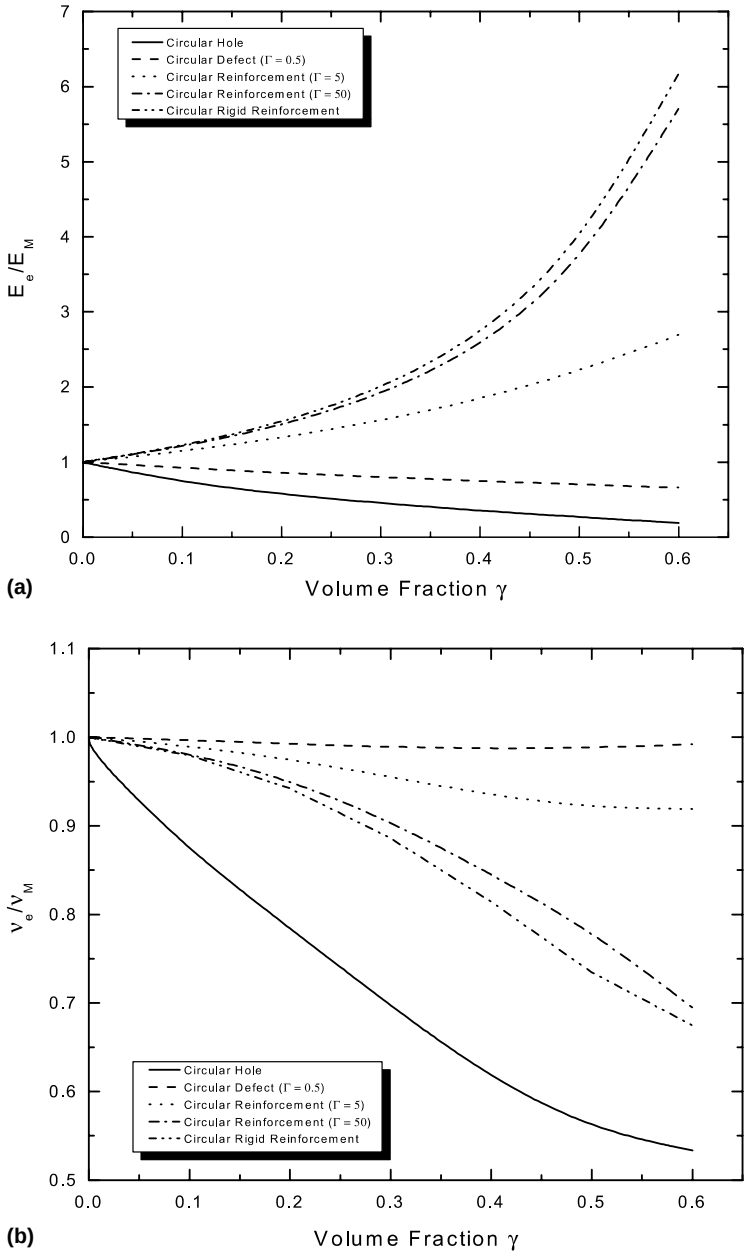

Fig. 8. Numerical results of the effective elastic modulus ratio E_e/E_M and Poisson's ratio v_e/v_M of the plates containing 9 (3×3) inhomogeneities versus different volume fraction γ: (a) E_e/E_M, (b) v_e/v_M.

From these numerical results, the arrangement of internal inhomogeneities has greatly influenced the mechanical behavior of the whole composite material, especially on the effective Poisson's ratio as shown in Figs. 12 and 13. Similarly, the effective Poisson's ratio varies greatly with different arrangements of internal inhomogeneities while the effective Young's modulus is relatively insensitive.

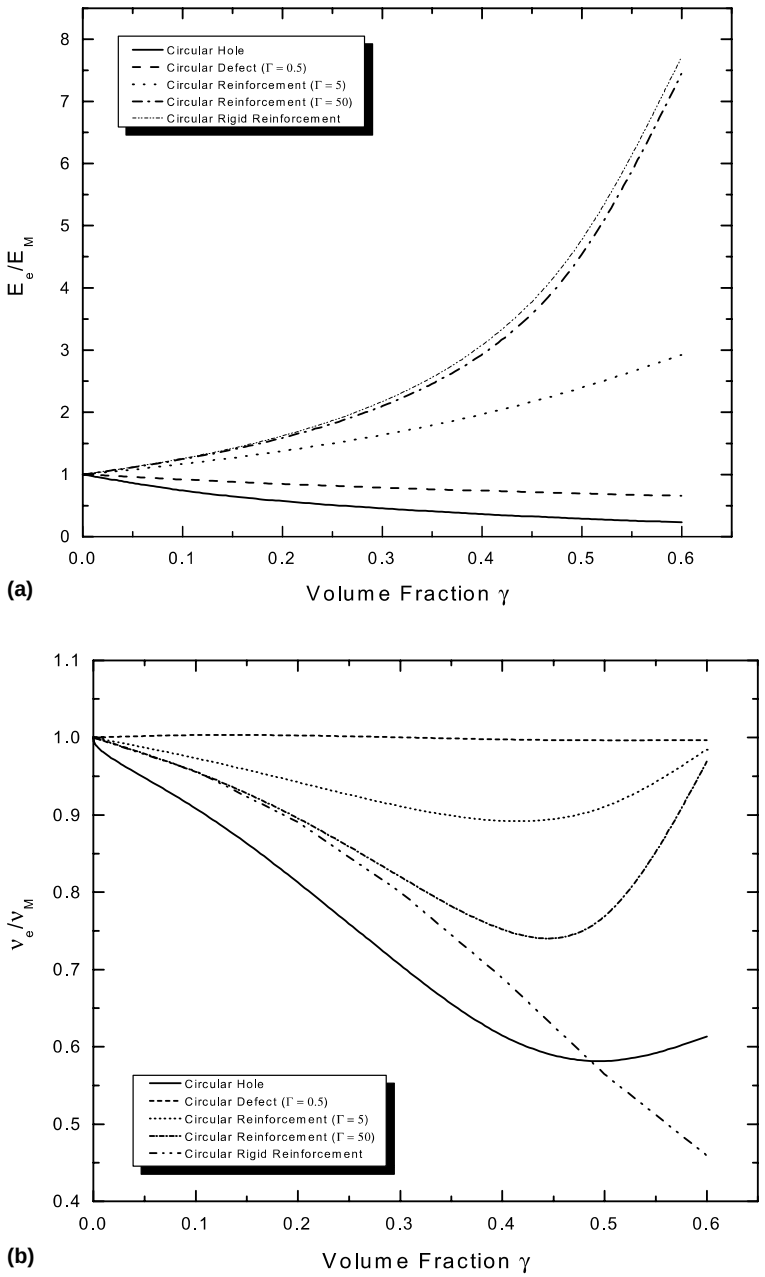

Fig. 9. Numerical results of the effective elastic modulus ratio E_e/E_M and Poisson's ratio v_e/v_M of the plates containing 100 (10×10) inhomogeneities versus different volume fraction γ: (a) E_e/E_M, (b) v_e/v_M.

4.2.2. Size effects with constant volume fractions between inhomogeneities and matrix

From the numerical results as shown in the previous section, the size effect of the internal inhomogeneities in the composites on the material response is significant and obviously cannot be neglected. At the constant volume fraction, several cases of square plates containing uniformly distributed inhomogeneities but

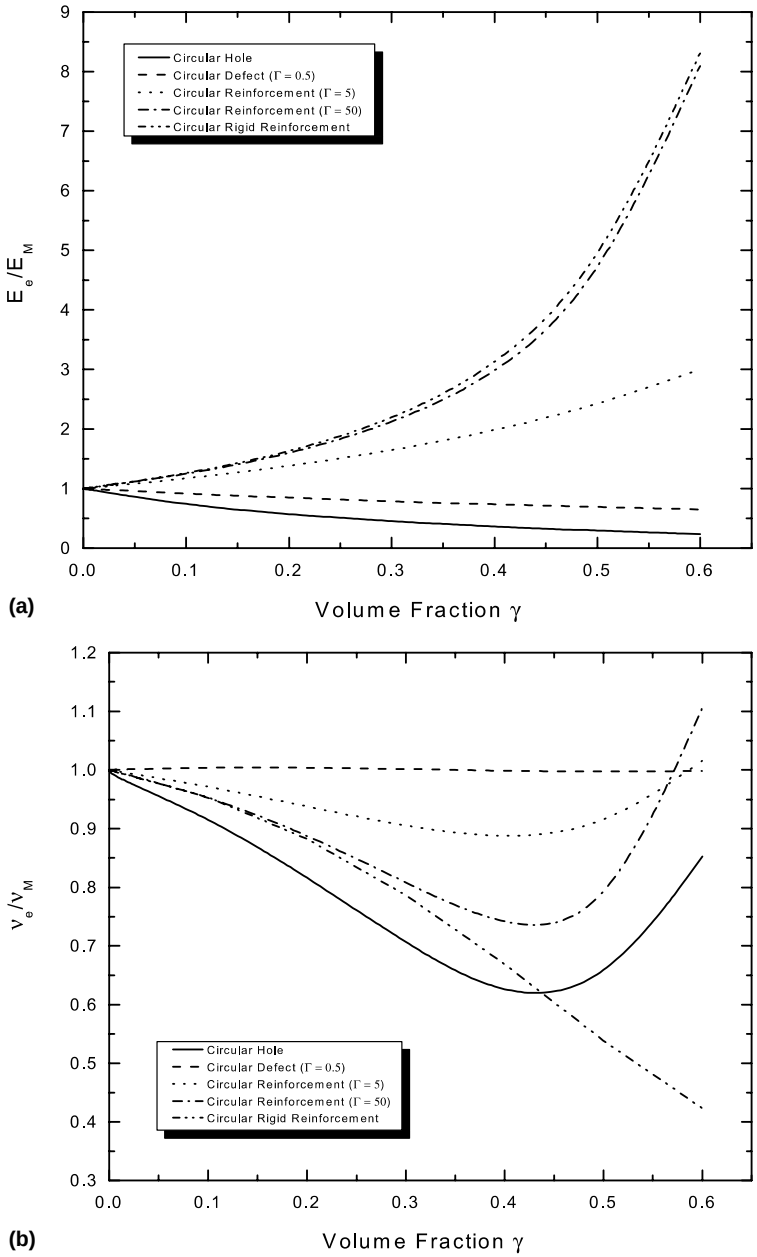

Fig. 10. Numerical results of the effective elastic modulus ratio E_e/E_M and Poisson's ratio v_e/v_M of the plates containing 400 (20×20) inhomogeneities versus different volume fraction γ: (a) E_e/E_M, (b) v_e/v_M.

with different numbers (including 1×1, 3×3, 5×5, 10×10, 20×20, 50×50 and 100×100) are considered again to identify the size effect.

The numerical results have been provided in Tables 4–8 for effective Young's moduli and Poisson's ratios with different internal inhomogeneities and different material properties. From these results, their variation

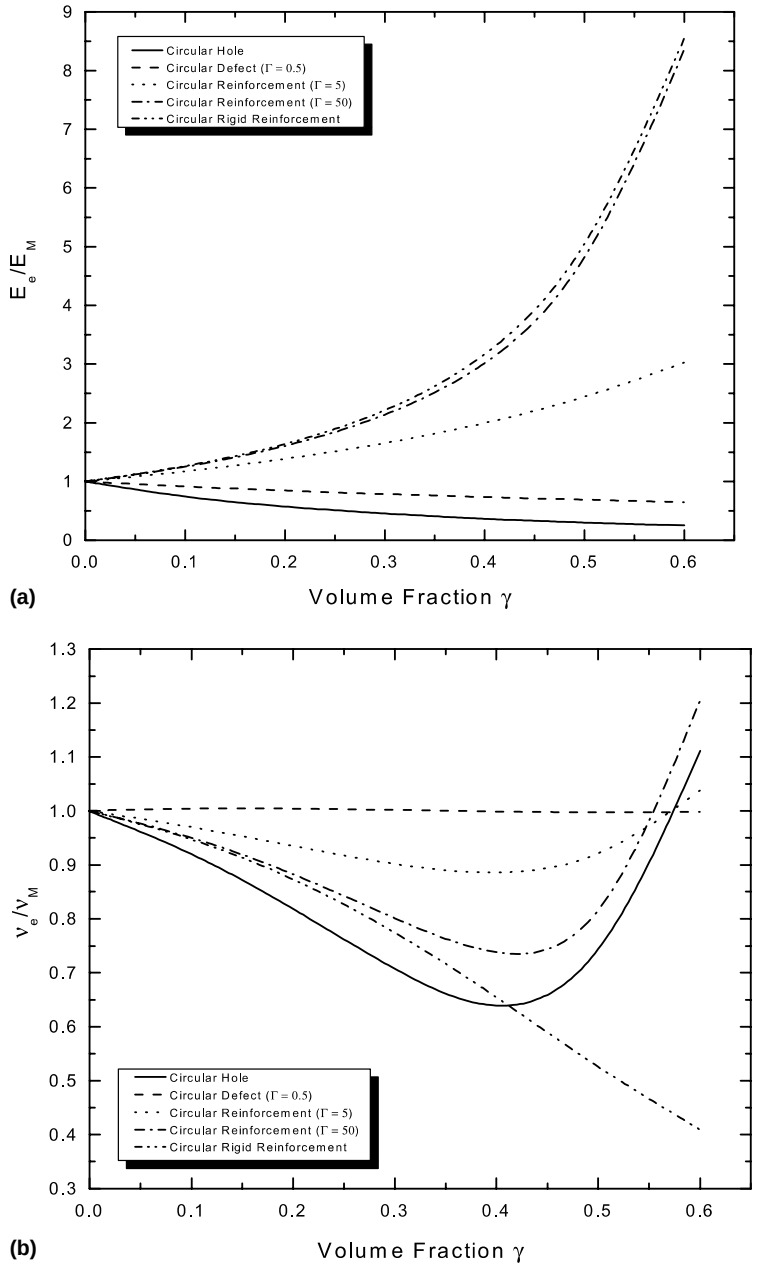

Fig. 11. Numerical results of the effective elastic modulus ratio E_e/E_M and Poisson's ratio v_e/v_M of the plates containing 10,000 (100×100) inhomogeneities versus different volume fraction γ: (a) E_e/E_M, (b) v_e/v_M.

with changing the number of the internal inhomogeneities and their material properties is quite remarkable, complex with the complicated behavior.

It is noted that the numerical results for v_e/v_M become unstable in all cases of relatively big internal inhomogeneities, especially with volume fraction γ of 0.5 or 0.6 due to the great influence and interference along the edges of the plates. However, the numerical results on E_e/E_M is kept stable in all analysis cases.

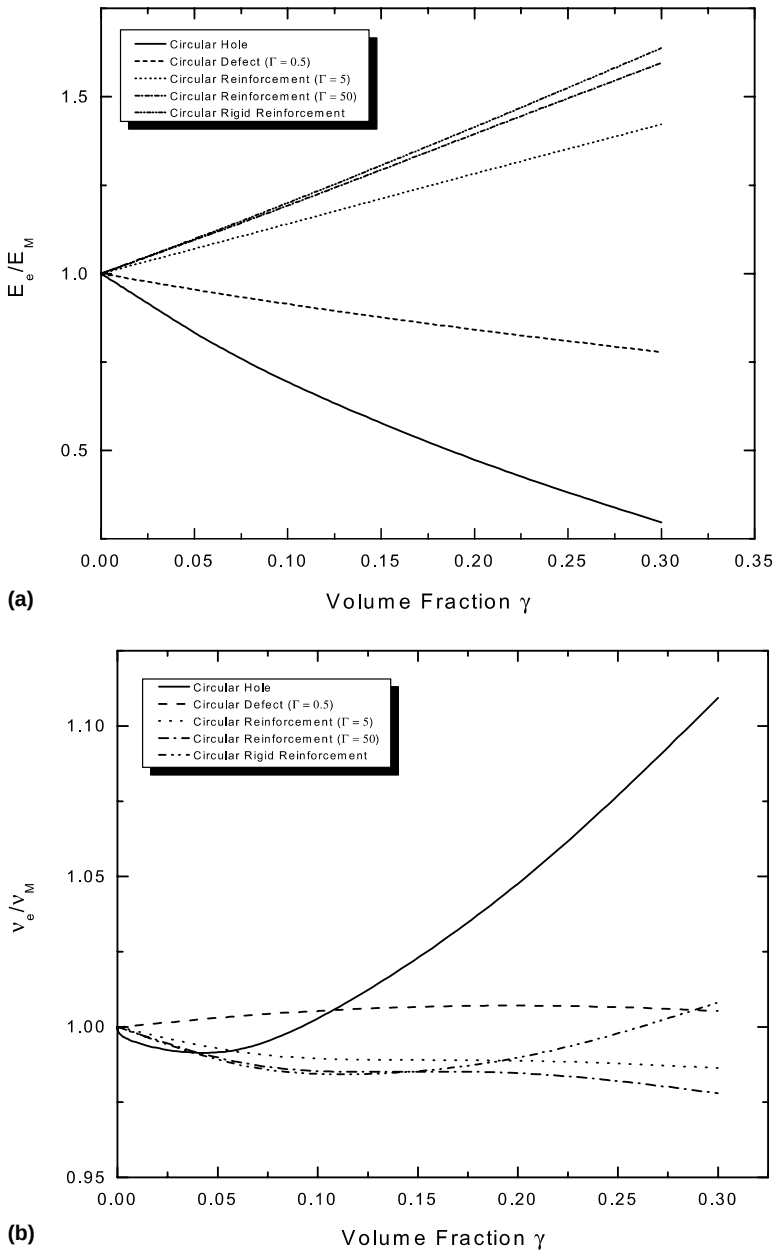

Fig. 12. Numerical results of the effective elastic modulus ratio E_e/E_M and Poisson's ratio v_e/v_M of the plates containing 41 inhomogeneities versus different volume fraction γ: (a) E_e/E_M, (b) v_e/v_M.

According to the results from the 1×1 meshes to the 100×100 meshes, the maximum discrepancies of the effective Young's moduli and Poisson ratios are 109.2% and 28.4% ($\Gamma = 0$); 7.7% and 7.6% ($\Gamma = 0.5$); 57.0% and 19.7% ($\Gamma = 5$); 220.0% and 47.1% ($\Gamma = 50$); 215.4% and 64.9% ($\Gamma = \infty$), respectively.

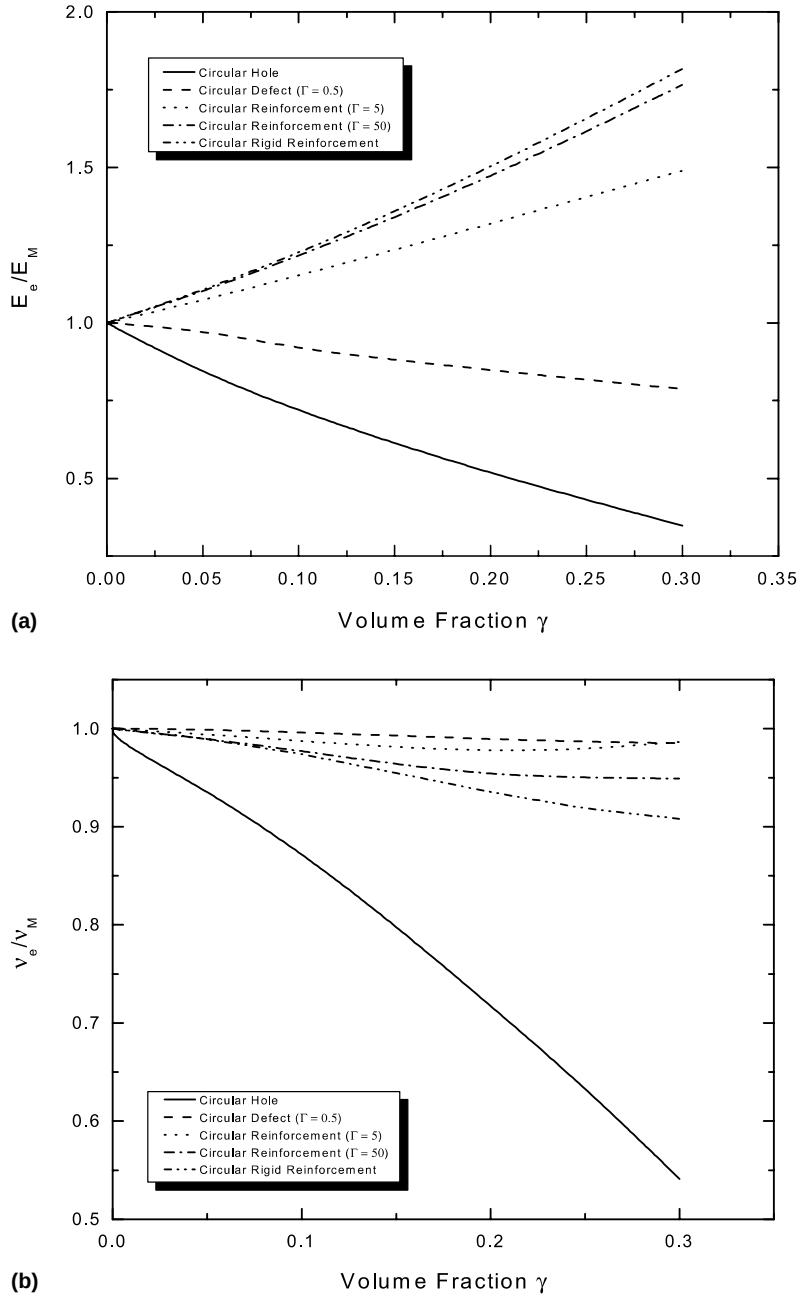

Fig. 13. Numerical results of the effective elastic modulus ratio E_e/E_M and Poisson's ratio v_e/v_M of the plates containing 16 inhomogeneities versus different volume fraction γ: (a) E_e/E_M, (b) v_e/v_M.

Consequently, the size effect on the effective Young's module and Poisson ratio are critical and the related material properties are quite different due to the different size of the internal defect.

Table 4
Size effects of effective Young's moduli and Poisson's ratios indicated by internal defects (circular holes: $\Gamma = 0$)

Volume fractions	Material constants	Mesh						
		1×1	3×3	5×5	10×10	20×20	50×50	100×100
0.1	E_e/E_M	0.7869	0.73259	0.72657	0.72436	0.72414	0.72433	0.72445
	v_e/v_M	0.7207	0.87076	0.89662	0.91312	0.9202	0.92403	0.92524
0.2	E_e/E_M	0.6108	0.57116	0.56652	0.5648	0.56467	0.56487	0.56498
	v_e/v_M	0.6593	0.78462	0.80377	0.81459	0.81843	0.82016	0.82064
0.3	E_e/E_M	0.4562	0.4504	0.44934	0.44907	0.44924	0.44947	0.44957
	v_e/v_M	0.6703	0.69628	0.70193	0.70398	0.70384	0.70328	0.70301
0.4	E_e/E_M	0.322	0.35263	0.35677	0.35943	0.36064	0.36135	0.36159
	v_e/v_M	0.752	0.61499	0.60433	0.60431	0.60754	0.61043	0.68527
0.5	E_e/E_M	0.2084	0.26703	0.27775	0.28701	0.29269	0.29641	0.29769
	v_e/v_M	0.8953	0.55721	0.52977	0.56791	0.62358	0.66867	0.68527
0.6	E_e/E_M	0.1208	0.1883	0.20445	0.22799	0.2378	0.24886	0.25267
	v_e/v_M	1.057	0.53364	0.48289	0.6135	0.85202	1.04279	1.1114

Table 5
Size effects of effective Young's moduli and Poisson's ratios indicated by internal defects (circular defect: $\Gamma = 0.5$)

Volume fractions	Material constants	Mesh						
		1×1	3×3	5×5	10×10	20×20	50×50	100×100
0.1	E_e/E_M	0.94987	0.92145	0.91743	0.91532	0.91462	0.91434	0.91427
	v_e/v_M	0.96399	0.99707	1.00155	1.00394	1.00477	1.00514	1.00524
0.2	E_e/E_M	0.89781	0.85508	0.84918	0.84618	0.8452	0.84481	0.84473
	v_e/v_M	0.94074	0.99261	0.99942	1.00294	1.0041	1.00459	1.00472
0.3	E_e/E_M	0.84604	0.79738	0.79072	0.78737	0.78629	0.78587	0.78577
	v_e/v_M	0.9311	0.98903	0.9966	1.00036	1.00152	1.00196	1.00206
0.4	E_e/E_M	0.79652	0.74692	0.74013	0.73665	0.73559	0.73517	0.73507
	v_e/v_M	0.93365	0.98702	0.99413	0.99745	0.99836	0.99864	0.99868
0.5	E_e/E_M	0.74869	0.70132	0.69475	0.6914	0.69035	0.68992	0.68984
	v_e/v_M	0.94781	0.988	0.9938	0.99633	0.9969	0.99698	0.99696
0.6	E_e/E_M	0.70279	0.6591	0.65309	0.6529	0.64901	0.64863	0.64854
	v_e/v_M	0.97069	0.99217	0.99628	0.99679	0.99829	0.99827	0.99822

5. Conclusions

This paper introduces a new approach to evaluate the effective material properties of composites with defect or reinforcement by utilizing a special finite element. According to the numerical results obtained in the present numerical analysis, the following important conclusions have been obtained from different effects of inhomogeneities in composite materials:

(1) The size effects indicated by the internal inhomogeneities in composite materials are very important and cannot be neglected. The numerical analysis using special defect/reinforcement finite elements developed is relatively simple, quite convenient while extremely effective and efficient for such problems, which has been mixed with the concept of effective plate.

Table 6
Size effects of effective Young's moduli and Poisson's ratios indicated by internal reinforcements (circular reinforcement: $\Gamma = 5$)

Volume fractions	Material constants	Mesh						
		1×1	3×3	5×5	10×10	20×20	50×50	100×100
0.1	E_e/E_M	1.07523	1.14257	1.15379	1.16005	1.16232	1.16332	1.1636
	v_e/v_M	1.04979	0.99016	0.98017	0.97447	0.97234	0.97133	0.97105
0.2	E_e/E_M	1.33703	1.32288	1.35052	1.36617	1.3721	1.37481	1.37549
	v_e/v_M	1.08706	0.97526	0.95471	0.94272	0.93817	0.93601	0.93541
0.3	E_e/E_M	1.29139	1.54903	1.59749	1.6254	1.63607	1.64099	1.64231
	v_e/v_M	1.10436	0.95513	0.92625	0.90942	0.90314	0.90024	0.89944
0.4	E_e/E_M	1.45624	1.83504	1.90886	1.95235	1.96815	1.97556	1.97766
	v_e/v_M	1.09467	0.9347	0.90397	0.88722	0.88172	0.87954	0.87902
0.5	E_e/E_M	1.66911	2.20774	2.31521	2.37845	2.40198	2.41334	2.41629
	v_e/v_M	1.04808	0.9203	0.90234	0.8979	0.89938	0.90165	0.90264
0.6	E_e/E_M	1.92608	2.69409	2.85753	2.92513	2.99861	3.01851	3.02416
	v_e/v_M	0.95482	0.91934	0.95093	0.98504	1.01615	1.03303	1.03886

Table 7
Size effects of effective Young's moduli and Poisson's ratios indicated by internal reinforcements (circular reinforcement: $\Gamma = 50$)

Volume fractions	Material constants	Mesh						
		1×1	3×3	5×5	10×10	20×20	50×50	100×100
0.1	E_e/E_M	1.10115	1.20032	1.21751	1.22725	1.23084	1.23245	1.23289
	v_e/v_M	1.06584	0.9824	0.96769	0.95916	0.95593	0.95439	0.95395
0.2	E_e/E_M	1.23298	1.48336	1.53191	1.56018	1.57116	1.57627	1.57758
	v_e/v_M	1.11617	0.95192	0.9186	0.89852	0.89069	0.88693	0.88587
0.3	E_e/E_M	1.41984	1.89162	1.99142	2.05121	2.07475	2.08583	2.08883
	v_e/v_M	1.13946	0.90512	0.85244	0.82012	0.80759	0.80168	0.80004
0.4	E_e/E_M	1.69893	2.51848	2.70743	2.82503	2.86943	2.89077	2.89691
	v_e/v_M	1.12474	0.84555	0.78001	0.74172	0.72859	0.72322	0.72191
0.5	E_e/E_M	2.09756	3.59966	3.99121	4.24603	4.34763	4.39888	4.41268
	v_e/v_M	1.05764	0.78126	0.73555	0.72551	0.73164	0.73952	0.74286
0.6	E_e/E_M	2.61274	5.71111	6.83063	7.45254	8.09705	8.30095	8.35969
	v_e/v_M	0.92408	0.69483	0.81471	0.9692	1.10595	1.18073	1.20604

(2) The arrangement and distribution of the internal inhomogeneities are also crucial, and thus the strength of the whole material would be changed remarkably even with the same volume fraction in contrast with the conjectures from conventional mechanics of composite materials.
(3) It is granted that the defects with softer materials will make the whole plates weaker and the reinforcements with harder material will make the whole plates stronger, but their variations are quite complex.
(4) Variation of the strength of the composites containing defect or reinforcement can be scaled using the effective material properties including the elastic modulus and the Poisson's ratio.

Table 8
Size effects of effective Young's moduli and Poisson's ratios indicated by internal reinforcements (circular rigid reinforcement: $\Gamma = \infty$)

Volume fractions	Material constants	Mesh						
		1×1	3×3	5×5	10×10	20×20	50×50	100×100
0.1	E_e/E_M	1.10434	1.21049	1.22705	1.23643	1.23994	1.24155	1.24201
	v_e/v_M	1.06801	0.97948	0.96511	0.95675	0.95354	0.95198	0.95152
0.2	E_e/E_M	1.24072	1.51692	1.56253	1.5892	1.59988	1.60505	1.60641
	v_e/v_M	1.12349	0.94229	0.91015	0.8906	0.88277	0.87886	0.87773
0.3	E_e/E_M	1.4337	1.96785	2.06209	2.11931	2.14281	2.15446	2.15776
	v_e/v_M	1.16102	0.88598	0.83338	0.80023	0.78668	0.77986	0.77785
0.4	E_e/E_M	1.72034	2.66523	2.84859	2.96586	3.01237	3.03618	3.04336
	v_e/v_M	1.18002	0.81439	0.73856	0.68942	0.6696	0.65968	0.65675
0.5	E_e/E_M	2.13348	3.85605	4.24246	4.49849	4.60497	4.66135	4.67715
	v_e/v_M	1.17792	0.73456	0.63164	0.56461	0.53829	0.52568	0.52221
0.6	E_e/E_M	2.71184	6.17832	7.20935	7.7247	8.31146	8.49708	8.55274
	v_e/v_M	1.1656	0.67451	0.53994	0.45924	0.42341	0.41179	0.40924

(5) On different scales of the internal defects or reinforcements, the size effect should be different due to the physical essence but the present finite element analysis based on the macro-mechanics is not able to show those differences in detail. Especially for nano-scale problems, there should be other approaches to set up further new models for numerical analysis based on the micro-mechanics.

Acknowledgments

This study was supported by the Brain Korea 21 project from the Ministry of Education in Korea. The authors would like to acknowledge their financial support during this work.

References

Andrievski, R.A., Glezer, A.M., 2001. Size effects in properties of nanomaterials. Scripta. Mater. 44, 1621–1624.
Budiansky, B., 1965. On the elastic moduli of heterogeneous materials. J. Mech. Phys. Solids 13, 223–227.
Benveniste, Y., Dvorak, G.J., Chen, T., 1989. Stress field in composites with coated inclusions. Mech. Mater. 7, 305–317.
Christensen, R.M., 1979. Mechanics of Composite Materials. John Wiley & Sons, New York.
Christensen, R.M., 1990. A critical evaluation for a class of micromechanics models. J. Mech. Phys. Solids 38, 379–404.
Eshelby, J.D., 1955. The elastic interaction of point defects. Acta Metall. 3, 487–490.
Fischer, H., Rentzsch, W., Marx, R., 2002. A modified size effect model for brittle nonmetallic materials. Eng. Fract. Mech. 69, 781–791.
Gibson, R.F., 1994. Principles of Composite Material Mechanics. McGraw-Hill, Singapore.
Hasin, Z., 1962. The elastic moduli of heterogeneous materials. J. Appl. Mech. 29, 143–150.
Hasin, Z., 1983. Analysis of composite materials—a survey. J. Appl. Mech. 50, 481–505.
Hill, R., 1965. A self consistent mechanics of composite materials. J. Mech. Phys. Solids 13, 213–222.
Meguid, S.A., Kalamkarov, A.L., 1994. Asymptotic homogenization of elastic composite materials with a regular structure. Int. J. Solids Struct. 31 (3), 303–316.
Meguid, S.A., Zhu, Z.H., 1995a. A novel finite element for treating inhomogeneous solids. Int. J. Numer. Meth. Eng. 38, 1579–1592.
Meguid, S.A., Zhu, Z.H., 1995b. Stress distribution in dissimilar materials containing inhomogeneities near the interface using a novel finite element. Finite Elem. Anal. Des. 20, 283–298.

Meng, Q., Zhang, T., Du, S., 2001. Boundary element method simulation of the size effect in particle dispersed composites. Comput. Struct. 79, 577–581.

Muskhelishvili, M.I., 1953. Some Basic Problems of the Theory of Elasticity. Nordhoff, Groningen, Holland.

Piltner, R., 1985. Special finite elements with holes and internal cracks. Int. J. Numer. Meth. Eng. 21, 1471–1485.

Roscoe, R., 1952. The viscosity of suspensions of rigid spheres. Brit. J. Appl. Phys. 3, 267.

Saouma, V.E., Natekar, D., Sbaizero, O., 2002. Nonlinear finite element analysis and size effect study in a metal-reinforced ceramics-composite. Mater. Sci. Eng. A 323, 129–137.

Soh, A.K., Long, Z.F., 1999. A high precision element with a central circular hole. Int. J. Solids Struct. 36 (35), 5485–5497.

Soh, A.K., Long, Z.F., 2000. Development of two-dimensional elements with a central circular hole. Comput. Meth. Appl. Mech. Eng. 188, 431–440.

Soh, A.K., Yang, C.H., 2004. Numerical modeling of the interactions between a macro-crack and micro-defects. Eng. Fract. Mech. 71 (2), 193–217.

Tong, P., 1977. A hybrid crack element for rectilinear anisotropic material. Int. J. Numer. Meth. Eng. 11, 377–403.

Timoshenko, S.P., Goodier, J.N., 1970. Theory of Elasticity, third ed. McGraw-Hill, New York.

Tong, P., Pian, T.H.H., Lasry, S.J., 1973. A hybrid-element approach to crack problems in plane elasticity. Int. J. Numer. Meth. Eng. 7, 297–308.

Vinson, J.R., Sierakowski, R.L., 1987. The Behavior of Structures Composed of Composite Materials. Martinus Nijhoff.

Yang, C.H., Soh, A.K., 2001. Special membrane elements with internal defects. In: Proceedings of First MIT Conference on Computational Fluid and Solid Mechanics. MIT, USA, pp. 554–558.

Yang, C.H., Soh, A.K., Hoon, K.H, 2003. Numerical modeling of the interactions between circular/elliptic/line inhomogeneities embedded in a matrix. Int. J. Nonlinear Sci. Numer. Simul. 4, 1–10.

Zhang, J., Katsube, N., 1995a. A hybrid finite element method for heterogeneous materials with randomly dispersed elastic inclusions. Finite Elem. Anal. Des. 19, 45–55.

Zhang, J., Katsube, N., 1995b. A hybrid finite element method for heterogeneous materials with randomly dispersed rigid inclusions. Int. J. Numer. Meth. Eng. 38, 1635–1653.